misoSR: <u>M</u>edical <u>I</u>mage <u>Iso</u>tropic <u>S</u>uper-Resolution <u>R</u>econstruction

Eric Van Reeth[*,1,2], Geetha Soujanya[2], Michaël Sdika[1], Frédéric Cervenansky[1], and Chueh Loo Poh[*,2]

[1]Université de Lyon, CREATIS ; CNRS UMR5220 ; Inserm U1044 ; INSA-Lyon ; Université Lyon 1, France.
[2]School of Chemical and Bioengineering, Nanyang Technological University, Singapore

Abstract

Isotropic volumetric acquisition in Magnetic Resonance Imaging (MRI) is often challenging. A large number of factors such as patient or physiological motion, signal-to-noise ratio (SNR), available static magnetic field B_0 and total scanning time limit the acquired resolution. Super-resolution (SR) is a post-processing technique that optimally combines several anisotropic scans into a single isotropic volume that was not - or could not be - acquired in practice. If necessary conditions are met, the resulting isotropic volume offers clear improvements over the initial acquisitions such as reduced partial volume effect, oblique visualization and improved sharpness and SNR. This paper details the misoSR implementation of a SR isotropic reconstruction algorithm using the Insight Toolkit Library (ITK) library. It is a generic implementation that reconstructs an isotropic volume from any number of anisotropic volumes acquired from any orientation. The algorithm takes advantage of the inputs header information to handle the different scans properties such as field of view (FOV), resolution parameters and orientation. Step by step details on the implementation are given, parameters are individually detailed, and results are shown on different applications as an example of SR reconstruction. The algorithm is hosted on the Creatis Virtual Imaging Platform (VIP), which allows users to run misoSR without having to install the software on their system.

1 Introduction

In magnetic resonance imaging (MRI), a large number of factors such as patient or physiological motion, signal-to-noise ratio (SNR), available static magnetic field B_0 and total

---

[*]Correspondence to: Eric Van Reeth, 20 Avenue Jean Capelle, 69100 Villeurbanne. E-mail: eric.van-reeth@creatis.insa-lyon.fr ; and to Chueh Loo Poh, School of Chemical and Bio-Engineering, Nanyang Technological University, Singapore. E-mail: clpoh@ntu.edu.sg

scanning time limit the acquired resolution. In order to reduce the acquisition time and increase the SNR, highly elongated voxels are usually acquired by increasing the slice thickness. This inevitably limits the accurate assessment of anatomical structures in the through-plane dimension, increases the partial volume effect (less contrast and more blur), penalizes oblique reconstructions and further processing such as structure segmentation, 3D modelling or registration. Super-resolution (SR) is a post-processing technique that optimally combines several anisotropic acquisitions of the same scene into a single isotropic volume that was not - or could not be - acquired in practice. If each acquisition provides independent information, which is the case when patient motion occurs or when different scanning planes are used, resolution enhancement is possible.

Unlike classic interpolation techniques (linear, cubic, zero-padding-interpolation), SR is able to add significant high-frequency content into the reconstructed volume and efficiently remove some aliasing that might be present in the initial images if the acquisition sampling does not meet the Nyquist criterion. Note that two types of resolution enhancement can theoretically be performed using SR, namely i) in-plane and ii) through-plane resolution enhancement.

The feasibility of in-plane improvement in MRI using SR remains a subject of controversy because of i) the inherent lack of high-frequency components acquired in the in-plane dimensions and ii) the fact that a shift in the in-plane dimension corresponds to a simple phase modulation in the acquired k-space [1]. This means that for two spatially shifted volumes with similar field-of-views (FOV), similar k-space points are sampled which does not meet the necessary observation independence criterion for resolution enhancement. Later studies have been performed to clarify this point [2, 3, 4].

On the other hand, through-plane resolution improvement, and in particular isotropic reconstruction, has been extensively and successfully applied to MRI in various contexts such as functional imaging [5, 6], volumetric imaging [7, 8], brain MRI [9, 10, 11]. Review articles can be found in [12, 13]. Various acquisition strategies have been compared in [14] to optimize the reconstruction. Combining orthogonal acquisitions provides an optimal sampling of the k-space and offers a good trade-off between resolution, signal-to-noise ratio, and acquisition time [15, 8].

This paper presents a generic implementation of a SR algorithm - misoSR - that reconstruct an isotropic volume from several observations. It can handle various acquisition protocols (number of inputs, volume orientation, different FOVs) since the implementation is based on the header information. The proposed algorithm is written in C++ and based on the Insight Toolkit (ITK) library [16]. It is uploaded on the Virtual Imaging Platform (VIP) [17] hosted at Creatis (vip.creatis.insa-lyon.fr), which allows users to run misoSR without system compatibility constraints.

This article starts by presenting the theory of SR, then details the implementation step by step and presents each individual parameter. Different working examples including the set of used parameters are given and limitations and perspectives are listed to conclude.

2 Theory

2.1 Image Acquisition Model

SR algorithms are based on an acquisition model given in Eq. 1 that links the observations Y_k to the high-resolution image X. Observations are considered displaced, blurred, down-sampled and noisy versions of the ideal and unknown high-resolution image:

$$Y_k = D_k B_k G_k X + V_k \ , \ k = \{1, \ldots, N\} \tag{1}$$

In this equation, N is the total number of observations, G_k is the geometric transformation operator that encompasses both the transformation due to the plane acquisition orientation and the motion between acquisitions. B_k is a space invariant 3-D point-spread function (PSF), D_k is the down-sampling operator from the high-resolution space to the observation space, and V_k is an additive zero mean Gaussian noise. It is assumed that the PSF (B_k) is separable and has a Gaussian profile in each dimension. The choice of a Gaussian PSF is motivated by the study of Greenspan et al. in which it is shown that such a model is able to produce high-quality reconstructions [9]. In the through-plane dimension, the variance (σ_t) of the PSF is usually chosen so that the full width at half maximum (FWHM) equals to the slice thickness (t), such as: $\sigma_t = \frac{t}{2.35}$. The PSF profile in this dimension is thus defined by:

$$\mathrm{PSF}_t(z) = \frac{1}{\sqrt{2\pi\sigma_t^2}} \exp\left(-\frac{z^2}{2\sigma_t^2}\right)$$

The in-plane PSF is constructed as a convolution of two identical Gaussian functions which variance is user defined.

2.1.1 Regularization

The general model given in Eq. 1 is reformulated as a regularized inverse problem because of its ill-posed nature. Let $\hat{Y}_k = D_k B_k G_k \hat{X}$ be the observations estimator, and $\Gamma_{TTV}(\hat{X})$ the regularization term:

$$X = \arg\min_{\hat{X}} \left[\sum_{k=1}^{N} \left\| Y_k - \hat{Y}_k \right\|_2^2 + \lambda \Gamma_{TTV}(\hat{X}) \right] \tag{2}$$

where λ balances the influence of the regularization term and the data fidelity term. The chosen regularization term prevents the apparition of noise by penalizing the L_1 norm of the magnitude of the image gradient, which favours the reconstruction of smooth images with sharp transitions [18]. Farsiu et al. introduced in [19] the bilateral-TV that proved to produce high-quality results and to be computationally efficient, which is an interesting consideration when processing large dataset. In misoSR, the bilateral-TV regularizer is extended to 3-D to match the dimension of the isotropic reconstruction

$$\hat{X}^{n+1} = \hat{X}^n + \gamma \times \frac{\beta^{n-1}}{N} \Big[\sum_{k=1}^{N} G_k^T B^T D_k^T (Y_k - \hat{Y}_k^n) - \lambda \sum_{\substack{l=-P \\ m=-P \\ n=0 \\ l+m+n \geq 0}}^{P} \alpha^{|m|+|l|+|n|} [\mathbf{Id} - S_{xyz}^{-(lmn)}] \operatorname{sgn}(\hat{X}^n - S_{xyz}^{lmn} \hat{X}^n) \Big]$$

(3)

problem. It is defined as:

$$\Gamma_{TTV}(X) = \sum_{\substack{-P \leq l \leq P \\ -P \leq m \leq P \\ 0 \leq n \leq P \\ l+m+n \geq 0}} \alpha^{|m|+|l|+|n|} ||X - S_{xyz}^{lmn} X||_1$$

In this equation, P is the size of the regularizer kernel, S_{xyz}^{lmn} is the global shift operator and regroups respectively the horizontal (S_x^l), vertical (S_y^m) and depth (S_z^n) circular shift operators. For example, (S_x^l) shifts X by l pixels in the x axis and allows the calculation of the gradient in this dimension. The scalar parameter $(0 < \alpha < 1)$ controls the influence of higher scales derivatives in the regularization term. In a 3D problem the choice of P has a significant impact on the computation time. If P is set to 1, the TTV operator can be viewed as the classical TV operator and α does not impact the regularization process.

2.1.2 Convergence

To iteratively converge towards the optimal estimation, a gradient descent algorithm is used as explicitly shown in Eq. 3. The step size γ is decreased at each iteration by the parameter β, $(0 < \beta \leq 1)$. Note that the step size is also normalized with respect to the number of inputs to facilitate convergence in case a large number of inputs are used. In Eq. 3, T represents the transpose operator, *sgn* the sign function and *Id* the identity matrix. A stable solution is considered to be reached when the difference between two successive iterations is below a pre-determined threshold which is detailed in section 3.3.

3 Implementation

In this section, the successive steps of the algorithm and their associated parameters are detailed.

3.1 Registration

Registration is a key step in the SR process and should be optimized with great care. It corresponds to the deformation operator G_k of Eq. 1 that estimates the displacement between successive acquisitions. As mentioned earlier, the first input volume specified in the option file is used as the rigid image and all subsequent inputs are registered to it. The output image will thus be reconstructed in the same position as Y_1. Note that

the choice of the rigid input might have an significant impact in some applications.

A multi-resolution scheme is used to improve speed, accuracy and robustness. For more details on the multi-resolution scheme, the reader is referred to [16]. The number of multi-resolution levels can be set. Setting it to one is equivalent to a normal registration strategy. To avoid divergence, the maximum step length can be set, together with the maximum number of iterations per resolution level. Convergence is considered reached when the difference between successive iterations is below a minimum step length or when the maximum iteration number is reached. Iteration details are output to monitor the registration convergence with the selected parameters. Having a look at it is strongly advised at least for first uses since it is hard to set default registration parameters robust to any applications.

The registration used in misoSR is a 6 degree-of-freedom rigid transformation, allowing 3D translations and 3D rotations since it is the most common transformation found in practice. This might be a limitation for some applications but deformable registration often requires fine tuning which we decided to let the user handle separately.

3.2 Image Modelling

This section explains how the different steps of imaging model of Eq. 1 are implemented, and details the parameters associated to each process.

3.2.1 Initialization

A first guess of the output image, $\hat{X}^0$, is performed by averaging all the inputs after they have been registered to the rigid image and linearly interpolated to the isotropic sample grid. We have noted that the choice of the initialization does not dramatically influence the reconstructed image but a clever choice might reduce the required iteration number.

3.2.2 Deformation

This step uses the result of the registration step where the deformation operators were calculated. Note that in the registration step, the displacement from position k to position 1 is estimated, which actually corresponds to the operator $G^T(k)\colon Y_k \to Y_1$ for $k = \{2, \ldots, N\}$. The current iteration estimation (in position 1), $\hat{X}^n$, is successively displaced with the operator G_k to match the k-th position. Note that G_1 is the identity operator.

3.2.3 PSF Filtering

The next step corresponds to the PSF filtering of each previously deformed image. The 3D Gaussian PSF function is defined in part 2.1. The PSF variance in all three dimensions can be set. It should be noted that when no in-plane resampling is performed, i.e. when all inputs have similar in-plane resolutions, a low variance ($\sigma_{IP} = 0.75$ px) is usually a good choice. The variance of the through-plane PSF is set by default so that the full width at half maximum (FWHM) equals the slice thickness. However, user can
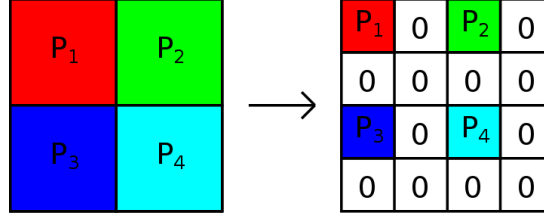
Figure 1: Illustration of the upsampling process used for error back-projection

change the through-plane PSF variance by tuning σ_{TP}, such as: FWHM $= \sigma_{TP} \times$ slice thickness.

3.2.4 Down-sampling

The last operator of the imaging model consists of down-sampling the current estimation to each of the observation sampling space. This operation is performed using a simple linear interpolation.

3.2.5 Error Computation

Successively applying the previously described operators allows to create the estimated observations: $\hat{Y}_k = D_k B_k G_k \hat{X}$ that lie in the same sampling space as the actual observations Y_k. In order to improve the current estimation at next iteration, the error, $e_k = Y_k - \hat{Y}_k$, is computed and back-projected into the high-resolution space as can be seen in Eq. 3.

3.2.6 Error Back-projection

The error back-projection step consists of applying the transform operators to the estimation error. It reverses the image acquisition process. The transform of the down-sampling operator is performed by upsampling e_k back to the isotropic sampling grid. Zero values are inserted in between known values as illustrated in Figure 1. For non-integer sampling factor, voxel values are linearly interpolated to match the isotropic grid positions.

The transform of the Gaussian blur operator is the blur operator itself. The same filtering that was applied for the error computation is applied to the upsampled error. Note that after upsampling, the number of zero-values present in the upsampled volume increases with the upsampling ratio. For this matter, the intensity values obtained after PSF filtering are normalized with respect to the through-plane to in-plane ratio.

Finally the displacement operator is inverted to move each error image back to the reference position (X) by applying: $G_k^T B_k^T D_k^T(e_k)$.

3.3 Stopping criterion

To stop the optimization process, a stopping criterion is set by the user (*tolerance*). When the difference between two successive iterations is less than the fixed threshold, the optimization process stops. The stopping criterion is normalized with respect to the difference between the first and second iteration. So if set to 0.03, process stops when the difference between the current and previous iterations is less than 3% of the difference between the initialization and the second iteration. In practice, this has proved to be a reliable method for most applications. At the end of each iteration, the value of this criterion is displayed for the user to monitor the convergence process. In parallel, the maximum number of iterations can also be set to avoid excessive running time.

4 Examples

This sections presents two examples of SR reconstruction based on misoSR. Both examples with inputs and parameter values can be found on VIP.

4.1 T2-weighted Rat Brain Data

4.1.1 Data

A first application of misoSR is shown in the context of T2-weighted rat brain images. Three orthogonal images are acquired in each anatomical plane on an horizontal MRI 4.7T Bruker Biospec with a surface quadrature receiving coil adapted to rat brain (Rapid Biomed). They are illustrated in Figure 2. The acquired voxel size is $0.1 \times 0.1 \times 0.5$ mm^3. A 2D multi-slice RARE sequence is used without slice gaps (TE=72.9 ms, TR>4.8 s depending on the number of slices needed to cover the whole brain). The TR is considered long enough for the longitudinal magnetization to recover. Acquisitions are triggered on the respiratory motion, and the animal is anaesthetized with isoflurane during the imaging process.

4.1.2 Reconstruction

An isotropic reconstruction was performed at a voxel size of $0.1 \times 0.1 \times 0.1$ mm^3 and is shown in Figure 2. The coronal image was used as the reference for the registration process. Note that a field inhomogeneity corrector is used as the only pre-processing step [22]. The parameters used for the reconstructions are listed in Table 1. Total computation was around 7 minutes on a 3.7Ghz, 8 cores machine. 13 iterations were needed for convergence. The full volume is $256 \times 128 \times 273$ pixels and can be downloaded from VIP for accurate evaluation.

Registration		Super-resolution	
Nb of multi-resolution	1	Output voxel size (in mm^3)	$0.1 \times 0.1 \times 0.1$
Max step length (in mm)	0.01	In-plane PSF (in px): σ_{IP}	0.65
Max iteration nb	600	Through-plane PSF: σ_{TP}	1
		Convergence step: γ	3
		Decreasing rate: β	0.9
		Regularizer weight: λ	1.25
		Regularizer nbhood: P	2
		Tolerance	0.005
		Max iteration nb	15

Table 1: Parameters used for the rat brain example

Axial ($0.1 \times 0.1 \times 0.5$ mm^3) Coronal ($0.1 \times 0.5 \times 0.1$ mm^3)

Sagittal ($0.5 \times 0.1 \times 0.1$ mm^3) SR Reconstruction ($0.1 \times 0.1 \times 0.1$ mm^3)
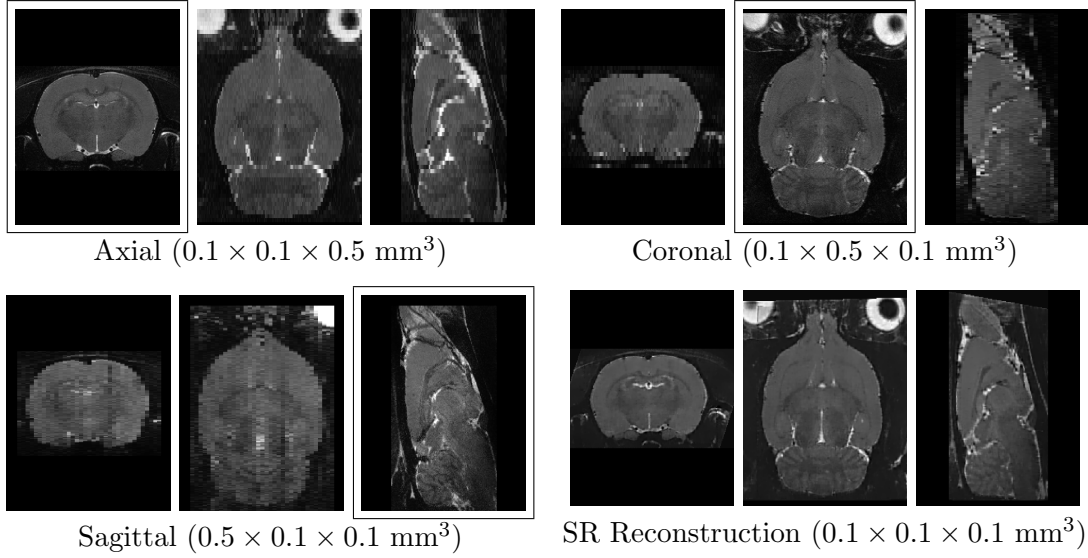
Figure 2: SR Reconstruction example on T2-weighted rat brain data. Boxed images show the original acquisitions ; the others are orthogonal reconstructions.

Registration		Super-resolution	
Nb of multi-resolution	3	Output voxel size (in mm^3)	$2.1 \times 2.1 \times 2.1$
Max step length (in mm)	1	In-plane PSF (in px): σ_{IP}	0.1
Max iteration nb	300	Through-plane PSF: σ_{TP}	1
		Convergence step: γ	3
		Decreasing rate: β	0.99
		Regularizer weight: λ	0.01
		Regularizer nbhood: P	2
		Tolerance	0.01
		Max iteration nb	15

Table 2: Parameters used for the lung example

4.2 Lung Data

4.2.1 Data

The second example of misoSR is on TWIST images of a lung cancer patient. 3D TWIST images are obtained in three orthogonal planes on a whole body Siemens Trio 3T MR scanner (Siemens Trio MRI scanner, Siemens Healthcare, Erlangen, Germany). The in-plane resolution of images is 2.1×2.1 mm^2 and the slice thickness is 7 mm with no slice gaps (TE= 0.8 ms, TR = 2.05 ms, FOV= 269 mm; Acquisition matrix = 128 x 128).

4.2.2 Reconstruction

An isotropic reconstruction of voxel size $2.1 \times 2.1 \times 2.1$ mm^3 is performed using misoSR. The coronal plane is taken as reference image for registration. All inputs are considered being at a similar phase of the breathing cycle. Orthogonal inputs and SR reconstruction are shown in Figure 3. The parameters used for registration and super-resolution are listed in Table 2. Total computation time was around 1 minute on 3.7 GHz, 8 cores machine to output a $128 \times 97 \times 120$ pixels volume in 10 iterations.

5 VIP implementation

5.1 Inputs - Outputs

Inputs are required to have correct header information. Standard image formats (Nifti, Dicom) are expected. Each input must be a single volumetric image.

The number of inputs used is up to the user. Using a single input is equivalent to single image interpolation with TV regularization and can be compared to classical interpolation methods (linear, cubic). A large input number will induce longer processing time but generally increases the reconstruction quality.

Note that the first input is taken as the reference image for the subsequent registration steps. Depending on the application, this can significantly influence the reconstruction.

Axial ($2.1 \times 2.1 \times 7.0$ mm^3) Coronal ($2.1 \times 7.0 \times 2.1$ mm^3)

Sagittal ($7.0 \times 2.1 \times 2.1$ mm^3) SR Reconstruction ($2.1 \times 2.1 \times 2.1$ mm^3)
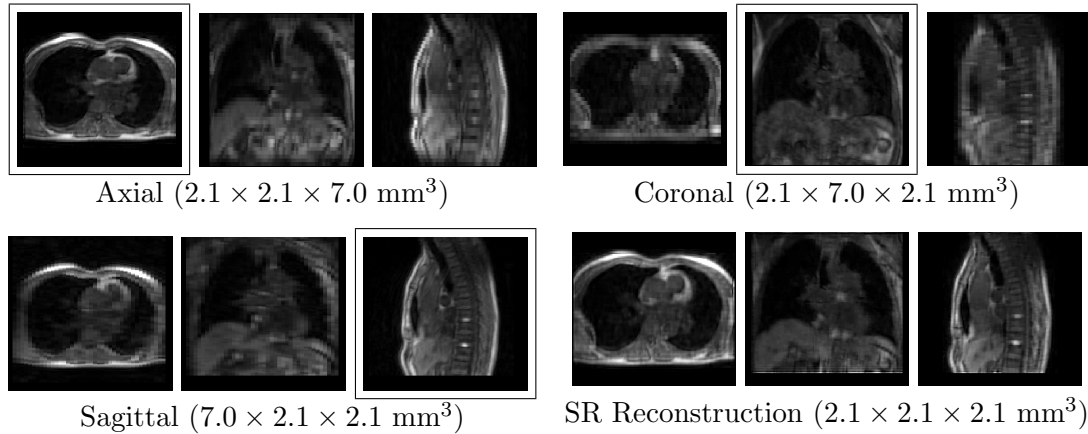
Figure 3: SR Reconstruction example on lung data. Boxed images show the original acquisitions ; the others are orthogonal reconstructions.

Inputs might have different resolutions. The output resolution of the SR volume is one of the parameters that has to be set by the user.

The result of the reconstruction is exported as a single Nifti volume. It can be read using for example the open-source software Fiji [20] or ITK-SNAP [21]. The output file is automatically placed in a folder corresponding to the date and time of the simulation. Finally, note that the orientation of the output file is set to the following matrix : (1 0 0 ; 0 1 0 ; 0 0 1). This usually causes the orientation of the output volume to be different from the orientation of the inputs.

5.2 Parameters summary

I/O:

Reference Image : The complete name (name + extension) of the image that will be used as a reference for the registration step.

Input Images : A single archive file (tar.gz) containing all volumes that will be used for the SR reconstruction. It must at least contain the file previously set as the reference image.

Registration:

Registration multi-res nb : Number of resolution levels used for registration

Registration max step size : Maximum step size (in mm) allowed for registration

Registration max iteration nb : Maximum iteration number allowed for registration at each resolution level

SR reconstruction:

Output voxel size : Voxel size (in mm) in each dimension of the output volume

SigmaIP : variance (in voxel) of the in-plane Gaussian PSF (see section 3.2.3)

SigmaTP : variance of the through-plane Gaussian PSF (section 3.2.3)

Beta : convergence step decreasing rate (Eq. 3)

Gamma : convergence step (Eq. 3)

Lambda : regularization weight (Eq. 3)

TV Neighborhood : regularizer neighborhood (P) (section 2.1.1)

Convergence tolerance : threshold under which convergence is considered reached (section 3.3)

Max SR iteration : Maximum iteration number allowed for SR reconstruction

Result directory : folder name in which the output will be placed

6   Discussion

This algorithm was originally developed on applications where only rigid registration was needed. For this reason, applications requiring deformable registration can not be directly used in misoSR. More generally, if the registration integrated in misoSR is not able to provide satisfactory results, registration tools like Elastix [23] can be used to pre-register all volumes. The resulting registered volumes can then be used as inputs in misoSR while setting the registration maximum number of iterations to 0.
A second restriction is the use of Gaussian PSF only. In some application like MRI, the slice selection profile might be better approximated using a box or a sinc function for example. Giving to the user the choice on the PSF profile in all 3 dimensions is part of future work.

The algorithm is currently available for external use through the VIP platform hosted at Creatis (vip.creatis.insa-lyon.fr). External users have to create an account and are allowed storage space to upload their data. Note that users are given administrator rights on their account, meaning that they can manage access rights to both their data and results. Unless users specify so, Creatis does not have access to the uploaded data and results.
Finally, we would like to remind the users that this algorithm should not be used for clinical nor commercial activities. It was developed and published for research purposes only. This is why the authors would appreciate that researchers cite this present article and VIP [17] whenever misoSR is used in their study.

7 Conclusion

This article describes misoSR, a new tool for isotropic reconstruction of medical images. One or more volumes representing the same scene are combined to produce a single high-resolution volume. Inputs are iteratively combined using an image acquisition model that comprises a rigid 6 degrees-of-freedom registration, a Gaussian PSF filtering and a down-sampling step. The overall reconstruction quality mainly depends on various factors :

- the image acquisition model accuracy (registration accuracy, PSF choice). Default parameters are advised in the option file but should be optimized for each application.

- the resampling factor. The reconstruction quality usually decreases when the initial voxels anisotropy increases. A study performed in [24, 8] illustrates this point and advises that anisotropy ratios higher than 5 should be avoided, i.e. slice thickness should not be more than 5 times than the in-plane pixel spacing. For high anisotropy ratios, it is usually hard to reduce the partial volume effect present in the initial scans.

- the initial scan orientations. Reconstruction quality increases when the redundancy between initial scans decreases. A denser coverage of the k-space logically leads to an optimal isotropic reconstruction, which explains why many studies combine orthogonal scans.

- the input homogeneity. It is important to keep in mind that the SR model assumes that all inputs provide the same information at similar spatial locations. Contrast in MRI can vary due to acquisition factors or field inhomogeneity. Important variations can thus alter the reconstruction procedure. Users might consider pre-processing such as field inhomogeneity corrections [22] before using misoSR.

Acknowledgements

References

[1] K. Scheffler, "Superresolution in mri?," *Magnet Reson Med*, vol. 48, no. 2, pp. 408–408, 2002.

[2] Q. M. Tieng, G. J. Cowin, D. C. Reutens, G. J. Galloway, and V. Vegh, "Mri demodulation frequency changes provide different information," *Magnet Reson Med*, vol. 66, no. 6, pp. 1513–1514, 2011.

[3] M. Uecker, T. J. Sumpf, and J. Frahm, "Reply to: Mri resolution enhancement: How useful are shifted images obtained by changing the demodulation frequency?," *Magnet Reson Med*, vol. 66, no. 6, pp. 1511–1512, 2011.

[4] Q. M. Tieng, G. J. Cowin, D. C. Reutens, G. J. Galloway, and V. Vegh, "Mri resolution enhancement: How useful are shifted images obtained by changing the demodulation frequency?," *Magnet Reson Med*, vol. 65, pp. 664–672, Mar. 2011.

[5] B. Scherrer, A. Gholipour, and S. Warfield, "Super-resolution reconstruction of diffusion-weighted images from distortion compensated orthogonal anisotropic acquisitions," in *IEEE Workshop on Mathematical Methods in Biomedical Image Analysis*, pp. 249 –254, jan. 2012.

[6] D. H. Poot, B. Jeurissen, Y. Bastiaensen, J. Veraart, W. Van Hecke, P. M. Parizel, and J. Sijbers, "Super-resolution for multislice diffusion tensor imaging," *Magnetic Resonance in Medicine*, vol. 69, no. 1, pp. 103–113, 2013.

[7] J. Woo, E. Murano, M. Stone, and J. Prince, "Reconstruction of high-resolution tongue volumes from mri," *IEEE T Bio-Med Eng*, vol. 59, pp. 3511 –3524, dec. 2012.

[8] E. Van Reeth, C. H. Tan, I. W. Tham, and C. L. Poh, "Isotropic reconstruction of a 4-d mri thoracic sequence using super-resolution," *Magnetic Resonance in Medicine*, 2014.

[9] H. Greenspan, G. Oz, N. Kiryati, and S. Peled, "Mri inter-slice reconstruction using super-resolution," *Magn Reson Imaging*, vol. 20, no. 5, pp. 437– 446, 2002.

[10] F. Rousseau, "A non-local approach for image super-resolution using intermodality priors," *Med Image Anal*, vol. 14, no. 4, pp. 594 – 605, 2010.

[11] A. Gholipour, J. A. Estroff, and S. K. Warfield, "Robust super-resolution volume reconstruction from slice acquisitions: Application to fetal brain mri," *IEEE T Med Imaging*, vol. 29, no. 10, pp. 1739–1758, 2010.

[12] H. Greenspan, "Super-resolution in medical imaging," *Comput J*, vol. 52, pp. 43–63, 2009.

[13] E. Van Reeth, I. W. K. Tham, C. H. Tan, and C. L. Poh, "Super-resolution in magnetic resonance imaging: A review," *Concept Magnetic Res - Part A*, vol. 40A, no. 6, pp. 306–325, 2012.

[14] R. Shilling, S. Ramamurthy, and M. Brummer, "Sampling strategies for super-resolution in multi-slice mri," in *15th IEEE International Conference on Image Processing*, (San Diego, California, USA), pp. 2240–2243, October 2008.

[15] E. Plenge, D. H. J. Poot, M. Bernsen, G. Kotek, G. Houston, P. Wielopolski, L. van der Weerd, W. J. Niessen, and E. Meijering, "Super-resolution methods in mri: Can they improve the trade-off between resolution, signal-to-noise ratio, and acquisition time?," *Magnet Reson Med*, vol. (), p. (), 2012.

[16] L. Ibanez, W. Schroeder, L. Ng, and J. Cates, *The ITK Software Guide*. Kitware, Inc., second ed., 2005. ISBN 1-930934-15-7.

[17] T. Glatard, C. Lartizien, B. Gibaud, R. Ferreira da Silva, G. Forestier, F. Cervenansky, M. Alessandrini, H. Benoit-Cattin, O. Bernard, S. Camarasu-Pop, N. Cerezo, P. Clarysse, A. Gaignard, P. Hugonnard, H. Liebgott, S. Marache, A. Marion, J. Montagnat, J. Tabary, and D. Friboulet, "A virtual imaging platform for multi-modality medical image simulation," *IEEE Transactions on Medical Imaging*, vol. 32, pp. 110–118, Jan 2013.

[18] L. Rudin, S. Osher, and E. Fatemi, "Nonlinear total variation based noise removal algorithms," *Physica D*, vol. 60, no. 1-4, pp. 259–268, 1992.

[19] S. Farsiu, M. D. Robinson, M. Elad, and P. Milanfar, "Fast and robust multiframe super resolution," *IEEE T Image Process*, vol. 13, no. 10, pp. 1327–1344, 2004.

[20] J. Schindelin, I. Arganda-Carreras, E. Frise, V. Kaynig, M. Longair, T. Pietzsch, S. Preibisch, C. Rueden, S. Saalfeld, B. Schmid, *et al.*, "Fiji: an open-source platform for biological-image analysis," *Nature methods*, vol. 9, no. 7, pp. 676–682, 2012.

[21] P. A. Yushkevich, J. Piven, H. Cody Hazlett, R. Gimpel Smith, S. Ho, J. C. Gee, and G. Gerig, "User-guided 3D active contour segmentation of anatomical structures: Significantly improved efficiency and reliability," *Neuroimage*, vol. 31, no. 3, pp. 1116–1128, 2006.

[22] N. Tustison, B. Avants, P. Cook, Y. Zheng, A. Egan, P. Yushkevich, and J. Gee, "N4itk: Improved n3 bias correction," *Medical Imaging, IEEE Transactions on*, vol. 29, pp. 1310–1320, June 2010.

[23] S. Klein, M. Staring, K. Murphy, M. a. Viergever, and J. P. W. Pluim, "Elastix: a toolbox for intensity-based medical image registration.," *IEEE Transactions on Medical Imaging*, vol. 29, pp. 196–205, Jan. 2010.

[24] E. Van Reeth, I. W. Tham, C. H. Tan, and C. L. Poh, "Phantom-based evaluation of isotropic reconstruction of 4-d mri volumes using super-resolution," in *IEEE Fourth International Workshop on Computational Intelligence in Medical Imaging (CIMI)*, pp. 6–13, IEEE, 2013.